Colloidal Nanocrystals of Zeolite β Stabilized in Alumina Matrix

M. V. Landau,*[,†,‡] D. Tavor,[†,‡] O. Regev,[‡] M. L. Kaliya,[†] and M. Herskowitz[†,‡]

The Blechner Center for Industrial Catalysis and Process Development and the Chemical Engineering Department, Ben-Gurion University of the Negev, Beer-Sheva, Israel

V. Valtchev and S. Mintova

Central Laboratory of Mineralogy and Crystallography, Bulgarian Academy of Sciences, Sofia, Bulgaria

Received November 12, 1998. Revised Manuscript Received April 22, 1999

Characteristics of zeolite β in stable aqueous colloidal solution were measured by cryo-TEM, DLS, SAXS and after separation from solution by SEM, HR-TEM. Twenty-nanometer spherical zeolite crystals were measured in equilibrium with flocculates. Mixing of colloidal zeolite solution with aluminogel yielded coagulation of both materials. The mass of zeolite adsorbed by aluminogel increased with decreasing pH. After calcination, pellets of the composite material at zeolite loading below 60 wt % contained separated nanocrystals of 10−15-nm zeolite β stabilized in the mesopores of alumina matrix. The imbedded zeolite had high structure order and acidity. No blocking of the zeolite micropores in composite materials was detected. The activity of zeolite β nanocrystals (imbedded in alumina matrix) in cumene cracking twice that of bulk nanozeolite clusters.

Introduction

Zeolite-based composite materials where the particles of zeolite phase are imbedded in inorganic or polymeric matrixes are widely applied in diverse areas, especially as catalysts, catalyst supports, and sorbents.[1] The matrix is normally a binder (Al_2O_3, $Al_2O_3-SiO_2$) for preparing strong pellets. Sometimes it displays catalytic activity. In case of nanocrystals zeolites[2] (<100 nm), the matrix impedes growth and aggregation of zeolite crystals. ZSM-5 nanocrystals were synthesized in mesopores of silica gel pellets using the matrix walls as a silica source for zeolite crystallization.[3,4] The product contained separated 25-nm zeolite nanocrystals inside the mesopores. However, inside the macropores and at the external surface of silica gel pellets, large zeolite crystals, >500 nm were formed.

Mixing the colloidal zeolite solution containing nanocrystals[2] with a sol or hydrogel of an inorganic matrix precursor followed by solid separation and thermotreatment is also employed. The size of zeolite crystals is determined during their preparation, provided a uniform distribution of zeolite nanocrystals in the mesoporous matrix volume is achieved. The zeolite particles in colloidal solutions behave close to pure silica.[5,6] It is negatively charged at pH > 5. The value of their ζ potential over pH range 10−12 is −40 to −60 mV.[5] Isoelectric point of aluminum hydroxide particles in water is pH ∼ 7.5.[6] Therefore, their ζ potential at higher pH values is much lower than for zeolite particles, but it strongly depends on the ionic strength of the solution. Increasing the salt concentration in water shifts the isoelectric point of aluminum hydroxide particles to pH values[7] ≥10. At high ionic strength, the aluminum hydroxide particles could remain positively charged up to pH = 13. Decreasing the pH to 10−12 at low ionic strength resulted in decrease of the negative charge on the aluminum hydroxide particles.[7] They could become positively charged depending on the pH and solution ionic strength while the zeolite particles remain highly negative. Therefore, progressive coagulation of colloidal zeolite particles in mixture with aluminogel could be expected as pH decreases due to increasing attractive forces between zeolite and aluminum hydroxide particles. Measurements of attractive forces between colloidal silica and alumina plate[8] or modified polymer films[9] in water demonstrated that such forces could be generated by electrostatic attraction between the oppositely charged surfaces and electrostatic repulsion between unequally charged negative surfaces. These

† The Blechner Center for Industrial Catalysis and Process Development.

‡ Chemical Engineering Department.

(1) Smirniotis, P. G.; Davydov, L.; Ruckenstein, E. *Catal. Rev.-Sci. Eng.* **1999**, *41* (1), 43.

(2) Lovallo, M. C.; Tsapatsis, M. In *Advanced Catalysts and Nanostructured Materials*; Modern Synthetic Methods; Moser, W. R., Ed., Academic Press: New York 1996; p 307.

(3) Landau, M. V.; Zaharur, N.; Herskowitz, M. *Appl. Catal.* **1994**, *A115*, L7.

(4) Landau, M. V.; Herskowitz, M. *Stud. Surf. Sci. Catal.* **1995**, *94*, 357.

(5) Schoeman, B. J. Synthesis and Properties of Colloidal Zeolite. Ph.D. Thesis, Goteborg, 1994.

(6) Brunelle, J. P. *Pure. Appl. Chem.* **1978**, *50*, 1211.

(7) Rowlands, W. N.; O'Brien, R. W.; Hunter, R. J.; Patrick, V. *J. Colloid Interface Sci.* **1997**, *188*, 325.

(8) Larson, I; Drummond, C. J.; C. Chan, D. Y.; Grieser, F. *Langmuir* **1997**, *13*, 2109.

(9) Zhang, J.; Uchida, E.; Suzuki, K.; Uyama, Y.; Ikada, Y. *J. Colloid Interface Sci.* **1996**, *178*, 371.

10.1021/cm980765u CCC: $18.00
Published on Web 07/22/1999

attractive forces could facilitate the adsorption of colloidal zeolite β particles by aluminogel. Uniform distribution of zeolite particles in the bulk of composite material after calcination could be expected due to adhesion between the zeolite nanocrystals and the aluminogel.

Mixing colloidal solution of zeolite L with a bohemite sol led to immediate coagulation which could be a result of attractive forces between oppositely charged zeolite and alumina particles.[2] A stable film of composite material, containing 93 wt % zeolite, displays uniform distribution of alumina, and no blockage of zeolite pores.[2] It is expected that at higher alumina content, the zeolite nanocrystals could be stabilized in the matrix with no aggregation. The purpose of this study is to present structural and morphological properties of colloidal zeolite β and composite material zeolite β−alumina obtained by mixing colloidal zeolite solution with aluminogel.

Experimental Section

Preparation of Zeolite *β*. Colloidal zeolite β crystals were synthesized from a clear solution containing 0.35 Na_2O:9.0 ROH:0.25 Al_2O_3:25 SiO_2:295 H_2O, where R is the organic template agent tetraethylammonium (TEA) (Sigma, 20% TEAOH in water). The silica source was derived from a colloidal silica suspension Bindzil 30/360 (Eka Nobel, Sweden, 31.1 wt % SiO_2, 0.6 wt % Na_2O). The suspension was freeze-dried to powder. The aluminum source was aluminum isopropylate (Sigma). No sodium was added from other sources. Distilled water was used in the preparation.

The silica solution was prepared by first dissolving the freeze-dried silica in a portion of the TEAOH solution then cooling to ambient temperature. The remaining TEAOH was used to dissolve the aluminum isopropylate to obtain a clear aluminate solution. The cold (ambient temperature) aluminate solution was added to the silica solution under intensive mixing. The clear mixture was transferred to a polypropylene reactor and submerged in an oil bath preheated to 100 °C. Synthesis solution was heat-treated at reflux without stirring. Liquid samples drawn at different crystallization times were separated by centrifugation (15 000 rpm). The solid samples were dried at 100 °C and analyzed by WAXS to determine the end of crystallization.

XRD analysis of the solid samples showed that a wide peak at $2\theta = 14-35°$ disappeared and the intensities of the peaks at $2\theta = 7.75$, 21.42, and 22.45° were stabilized. The crystallization was stopped after 12 days. Zeolite concentration in the mother liquor was 10.5 wt %. The solid was dried at 100 °C and calcined at 550 °C in air. EDX analysis of calcined solid material yielded Si/Al and Na/Al ratio of 16.9 and 0.15, respectively. Further heating of mother liquor for 2−3 days did not change the XRD patterns and composition of zeolite phase while the colloidal particles (DLS) were bigger. The mother liquor containing zeolite phase after heating for 12 days at 100 °C and cooling to room temperature was used in preparation of zeolite−alumina composites or bulk zeolite phase by evaporation.

Preparation of Aluminogel. An $Al(NO_3)_3$ (Fluka) aqueous solution (0.2 L, 1 M) was mixed with 0.1 L of distilled water in a 2.5-L volume flask. The solution was heated to 70 °C, and 15% aqueous NH_4OH (Frutarom) solution was slowly added under stirring to pH of 7.5. Then, 1 M $Al(NO_3)_3$ solution was slowly added until a pH of 9.5 was obtained (2 L mixture), stirred for 1 h at 70 °C, and aged at room temperature for 15 h. The $Al(NO_3)_3$ precipitate was separated from the suspension by filtration and washed with 2 L of distilled water per 50 g of Al_2O_3 to remove NO_3^- ions. The aluminogel was stored as a cake with 15 wt % Al_2O_3. The alumina concentration in the cake was calculated on the basis of its weight loss after drying at 100 °C for 3 h and calcination in air at 550 °C for 5 h.

Preparation of Composite Materials. The aluminogel cake was repulped in distilled water so that the alumina concentration in suspension was 2.5 wt %. The pH of the suspension was 9.05. A total of 35 g of this alumina hydroxide suspension was mixed at room temperature with 8.4 g of as-synthesized zeolite β colloidal solution at pH = 12.7 to reach Al_2O_3/zeolite weight ratio in the mixture of 1:1 and pH of 11.8. After stirring for 2 h, the mixture was aged at room temperature for 24 h without stirring. The precipitate was separated by decantation and dried under vacuum at 50 °C to reach 70 wt % water content. Pellets were formed by extrusion and dried in air at 120 °C for 5 h. The temperature was increased at 1°C/min, keeping it constant for 2 h at each of 200, 300, and 400 °C, and for 3 h at 550 °C. Two batches were prepared as described above, adjusting the pH of the suspension immediately after mixing to 11.0 and 10.0 by addition of diluted nitric acid. Composites with Al_2O_3/zeolite ratio < 1 were prepared as described above from aluminogel−zeolite mixtures with higher zeolite concentration adjusting the pH to 10.0 immediately after mixing.

Characterization. Wide-angle XRD (WAXS) patterns were measured on a Phillips difractometer PW 1050/70 (Cu K_α radiation) with graphite monochromator. Data were recorded at 0.02° step size with 2-s intervals. The peak positions and the instrumental peak broadening (β) were determined using silicon powder XRD Spacing (NIST standard reference material 640b). The crystal domains size was determined using Scherrer equation: $l = K\lambda/[(B^2 - \beta^2)^{0.5} \cos(2\theta/2)]$, where $K = 1.000$; $\lambda = 0.154$ nm; and B is the peak broadening at $2\theta = 22.45-22.55°$.

Small-angle X-ray scattering (SAXS) patterns were measured with Ni-filtered Cu Kα radiation (SEIFERT ID 3000 generator), which was shone through an evacuated compact Kratky camera (Anton PAAR) on the sample (liquid or powder), which was placed in a 1.5-mm diameter glass capillary (GLAS). A linear position-sensitive detector (MBRAUN) was used to record the scattering patterns. The sample-to-detector distance was 274 mm.

Infrared spectra were recorded by a Nicolet Impact 410 FTIR spectrometer using the KBr pellets (0.005 g sample and 0.1 g KBr), a scan number of 36, and a resolution of 2 cm^{-1}. The particle size distribution for zeolite colloidal solution was determined by dynamic light scattering (DLS) using Brookhaven Instruments ZetaPlus with 4-mW diode laser operating at 670 nm and fixed scattering angle of 90°.

Room-temperature ^{29}Si NMR spectra of solid samples were recorded at magic angle spinning (MAS) conditions on Bruker DSX-300 spectrometer operating at 59.6 MHz. Zirconia rotors (7 mm) spun at 4 kHz were used. The spectra were recorded by single pulse (SP) exitation. The recycle time for SP spectra was 30 s. A line broadening parameter of LB = 20 Hz was used. The chemical shift scale was related to δ (TMS = 0). A JEM-35 scanning electron microscopy (SEM), link system AN-1000, equipped with Si−Li detector was used.

Cryo-TEM micrographs of colloidal zeolite solution were recorded on a JEOL 1200EXII microscope equipped with a Gatan cold stage under an acceleration voltage of 100 kV in the conventional TEM mode. A nominal underfocus of about 4 μm was used. The images were recorded at −170 °C on Kodak SO-163 film developed in full strength D-19 developer for 12 min at room temperature. The specimens were prepared by deposition of a 5-μL solution on a TEM lacey carbon grid (Ted Pella Inc.). After blotting the grid, a thin (20−200 nm) film of the solution, suspended over its holes, was formed. The specimen was vitrified by plunging it into liquid ethane at its boiling point and transferred to the microscope under liquid nitrogen.

Zeolites and composite materials samples for high-resolution TEM (HR-TEM) were prepared by depositing a drop of an ultrasonicated aqueous suspension on a carbon-coated Cu grid. The grid was dried at 100 °C and mounted on a specimen holder. Micrographs were recorded using JEM 2010 microscope operated at 200 kV equipped with linked EDS. EDAX was performed in STEM mode to obtain the Si/Al ratio in the sample at spot size from 100 to 5 nm. Nanocrystals of zeolite

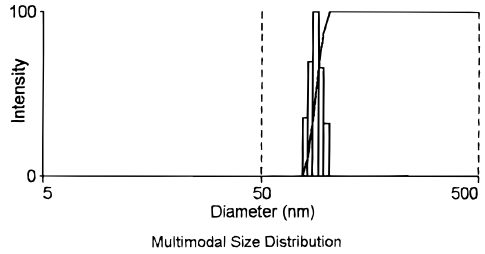

Figure 1. Stokes diameter distribution determined by DLS for diluted zeolite β colloidal solution (average value of five data points).

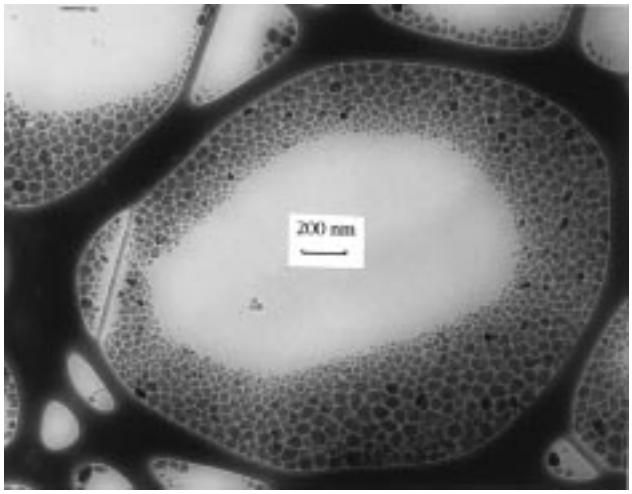

Figure 2. Cryo-TEM micrograph of a vitrified sample of colloidal zeolite β solution (bar = 200 nm).

β were radiation-sensitive, resulting in orientation change or structure degradation. Therefore, focusing was made in a sacrificial zone and the image was taken in an adjacent region.

N_2 adsorption−desorption isotherms were measured at liquid nitrogen temperature with a NOVA-1000 (Quantachrome, Version 5.01) instrument. Surface areas, total pore volumes, and pore size distributions were obtained from these isotherms using BET and BJH methods. Dried, as-synthesized zeolite samples were outgassed under vacuum at 100 °C, and calcined at 250 °C.

Acidity Test. Acidity of zeolite materials was determined indirectly measuring cumene conversion in a fixed-bed reactor at standard conditions: T = 360 °C, WHSV = 5.5 h^{-1}. Two grams of catalysts pellets (20−40 mesh) was loaded between silica gel layers in a stainless steel tubular reactor (21 mm i.d.). The reactor and preheater were heated electrically and controlled independently by Eurotherm controllers. The temperature was measured by chromel−alumel thermocoples inserted in a central thermowell. Cumene (Aldrich, 99% purity) was fed to the reactor inlet by a syringe pump (Razel Inc.). Nitrogen (Maxima, 99.9% purity) flow to the preheater inlet was 60 mL/min, controlled by Brooks 5850S mass flow controller. Propylene concentration in effluent gas flow was measured by on-line GC (Gow-Mac 580) equipped with packed HayeSep Q column (Sigma), 80/100 mesh, 8 ft × 1/8 in. × 0.065 in.

Results and Discussion

The State of Zeolite β in Colloidal Solution. The particle size distribution in diluted mother liquor, measured by DLS for large particles (>50 nm) is shown in Figure 1. Micrograph from cryo-TEM is displayed in Figure 2. The suspended film in a cryo-TEM specimen possesses a meniscus[10] and hence the film thickness is narrower in the center. Indeed, small, 10−20 nm particles are observed close to the center, apparently

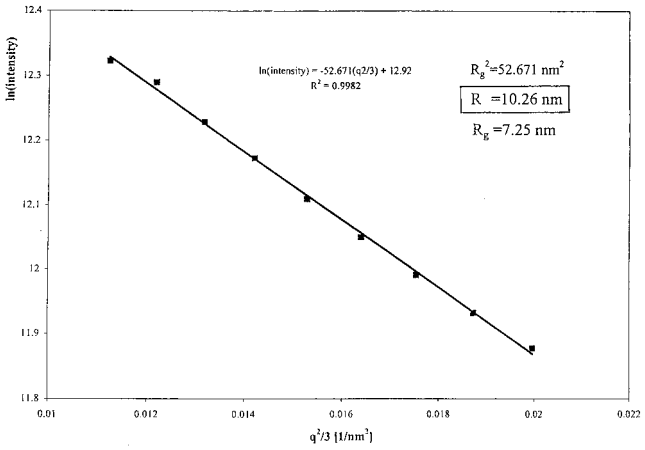

Figure 3. Guinier analysis of SAXS pattern of zeolite β colloidal solution.

zeolite nanocrystals. Larger, 60−100 nm particles, with a very rough surface texture were found closer to the boundary. Most of the zeolite material in colloidal solution exists in form of large particles, 60−100 nm, in agreement with DLS data. The shape and texture of large and intermediate particles (>20 nm) shown in Figure 2 are most probably aggregates of small zeolite nanocrystals 10−20 nm. These aggregates could be either water-rich flocculates or partially accreted crystals.

SAXS spectra of colloidal solution were analyzed using the Guinier approximation[11] assuming a noninteracting and globular pattern. Guinier analysis of the scattering curve of the colloidal solution is shown in Figure 3. On the basis of this analysis R_g of 7.25 nm was obtained. It corresponds to an average particle diameter[11] of 20.52 nm, in agreement with cryo-TEM data. Therefore, large particles are probably water-rich flocculates. Hence, the single 20-nm zeolite nanocrystals in the flocculates could be dispersed, by a proper procedure, in a mesoporous matrix.

The State of Bulk Zeolite β Separated from Colloidal Solution. SEM micrographs display dense packing of nearly spherical particles in the range of 60−100 nm, corresponding to the aggregate diameter in the parent colloidal solution from DLS and cryo-TEM data. The HR-TEM micrograph in Figure 4a indicates that those spherical particles are not single zeolite monocrystals but clusters of spherical 15−20 nm zeolite nanocrystals, in agreement with the smallest particles detected by cryo-TEM and SAXS in the colloidal solution. Macropores (>50 nm) in Figure 4a represent the void volume between the spherical clusters of zeolite nanocrystals detected by SEM.

The material contained few micropores (Table 1) in agreement with results presented elsewhere.[12,13] Most of its pore volume (0.52 cm^3/g) is in 10−25 nm mesopores (Figure 5, curve a) representing the void volume between zeolite nanocrystals inside clusters. It also

(10) Harwigsson, I.; Söderman, O.; Regev, O. *Langmuir* **1994**, *10*, 4731.
(11) Guinier, A.; Fournet, G. *Small Angle Scattering of X-rays*; Wiley-Interscience: New York, 1955.
(12) Cambor, M. A.; Corma, A.; Mifsud, A.; Perez-Pariente, J.; Valencia, S. *Stud. Surf. Sci. Catal.* **1997**, *105*, 341.
(13) Cambor, M. A.; Corma, A.; Valencia, A. *Microporous Mesoporous Mater.* **1998**, *25*, 59.

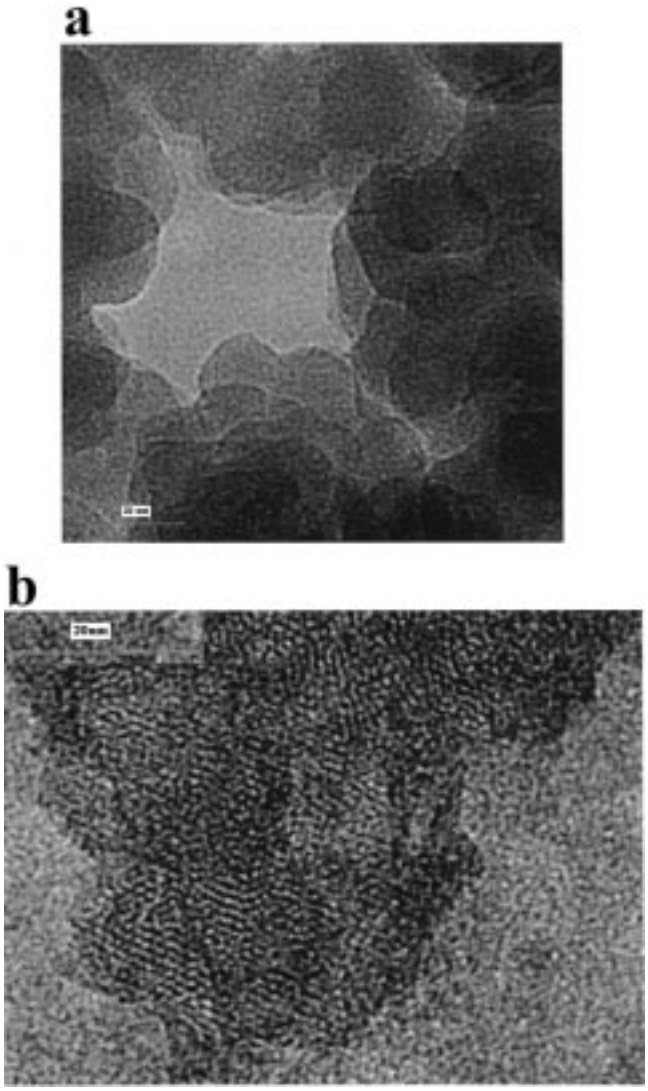

Figure 4. HR-TEM micrographs of zeolite β separated from colloidal solution (bar = 20 nm): (a) after drying at 100 °C and (b) after drying and calcination at 550 °C.

Table 1. N_2 Adsorption Properties of Colloidal Zeolite β, Alumina Matrix, and Composite Material

sample	surface area, m^2/g BET	surface area, m^2/g t-plot (ads.)	micropore vol ($P/P_o \leq 0.01$), cm^3/g	total pore vol (BJH, des.), cm^3/g
as-synthesized colloidal β (100 °C)	278	290	0.009	0.52
calcined colloidal β (550 °C)	646	300	0.165	0.68
Al_2O_3 matrix (550 °C)	320	–	0.039	0.60
48 wt % colloidal β–Al_2O_3 (550 °C)	473	–	0.120	0.80

contains 2–5 nm mesopores (Figure 5, curve a), accounting for the areas inside clusters with higher packing density of zeolite nanocrystals. The BET and t-plot surface area of the as-synthesized sample corresponds to the external surface of the crystallites blocked by TEA (in agreement with results reported[12,13] for zeolite β separated from colloidal solution and dried at 100 °C). It corresponds to a crystal size of 11 nm, calculated assuming spherical solid particles morphology, close to HR-TEM (Figure 4a), indicating minimal

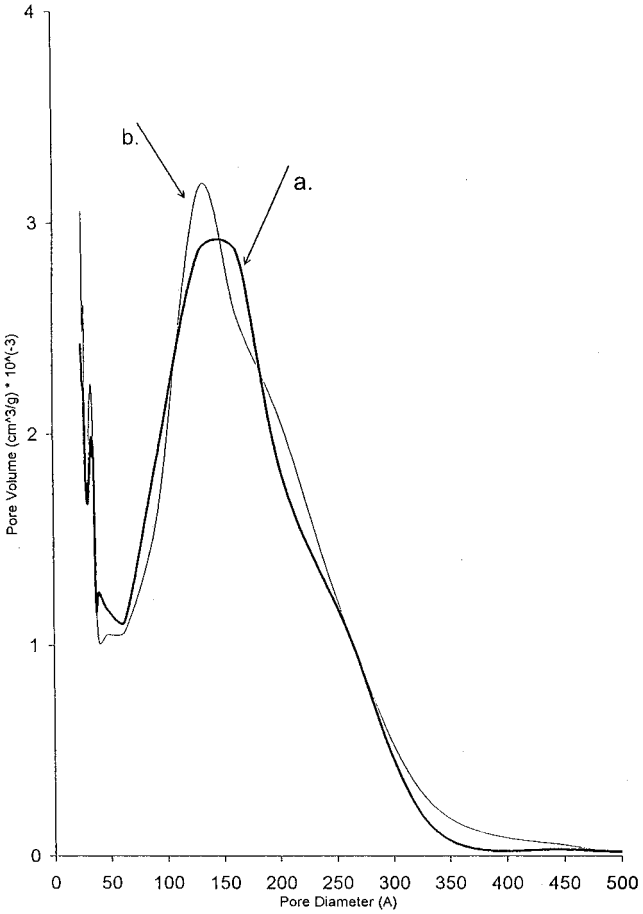

Figure 5. Pore size distribution curves calculated from desorption branch of the nitrogen sorption isotherm using Barret–Joyner–Halenda formula: (a) as synthesized zeolite β separated from colloidal solution and dried at 100 °C and (b) zeolite β separated from colloidal solution, dried and calcined at 550 °C.

contact between nanocrystals inside the clusters. These results are evident for aggregation of zeolite β spherical nanocrystals after separation from colloidal solution forming bulk spherial clusters with meso- and macropores between the primary zeolite crystals.

Zeolite Adsorption by Aluminogel. Calcined pellets of the precipitate obtained at pH = 11.8 contained 28 wt % zeolite, as measured by EDAX. The concentration of aluminum oxide phase (from aluminogel) in the solid obtained from colloidal suspension, separated by decantation, was 2.5 wt %. Since colloidal zeolite particles do not precipitate at this pH in a separate solution, these results could indicate adsorption of zeolite nanocrystals or their clusters by aluminogel. Furthermore, the zeolite content in the precipitate increased with decreasing the pH of the mixture. At pH = 10, most of the zeolite introduced to the mixture appeared in precipitate. The relative amount of zeolite adsorbed by aluminogel calculated by the zeolite content in precipitate was 56, 83, and 97% at pH = 11.8, 11.0, and 10.0, respectively.

Distribution of Zeolite Nanocrystals in Alumina Matrix. HR-TEM micrographs of pellets prepared at pH = 10, containing 48 wt % zeolite β (Figure 6a,b), show separate spherical zeolite nanocrystals with well-defined images of atomic layers (successive planes,

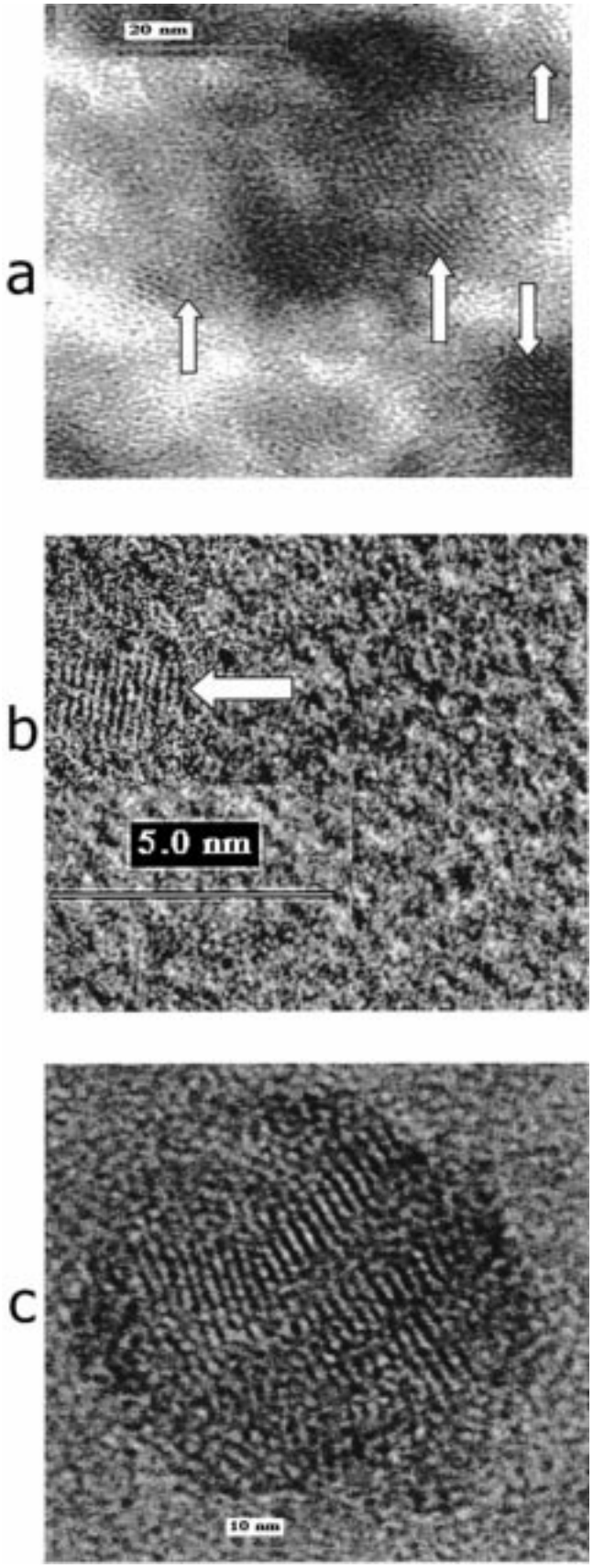

Figure 6. HR-TEM micrographs of calcined pellets of zeolite β−alumina composite materials: (a) 48 wt % zeolite−Al_2O_3, scale bar = 20 nm; (b) 48 wt % zeolite −Al_3O_3, scale bar = 5 nm; and (c) 80wt % zeolite−Al_2O_3, scale bar = 10 nm.

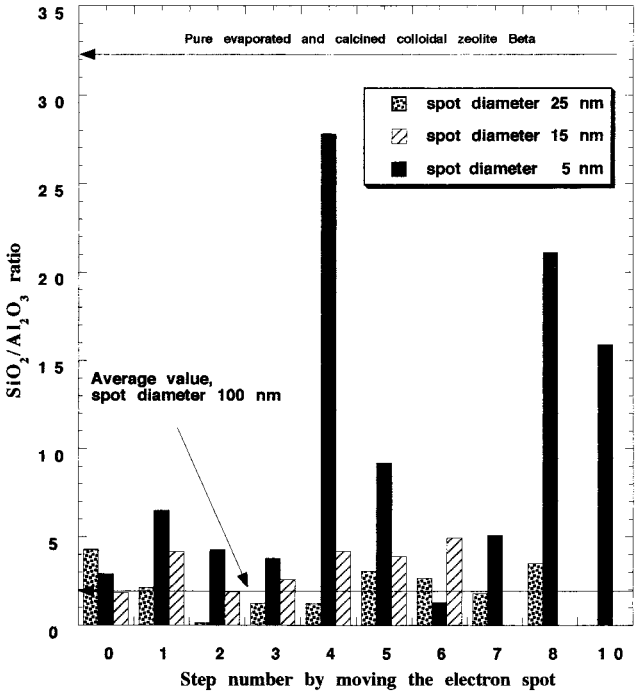

Figure 7. Effect of spot diameter on the SiO_2/Al_2O_3 ratio measured by EDAX in 48wt % zeolite β−Al_2O_3 composite material moving the electronic spot along the sample.

~1.32 nm characteristic of zeolite β[14]) ranging in dimensions from 5 to 15 nm. EDAX analysis of Si/Al atomic ratio was performed by moving the electronic spot along the sample in steps of 100−5 nm. The results in Figure 7 indicate significant jumps of the measured Si/Al ratio when the diameter of electron spot was decreased to 5 nm. At a spot diameter substantially wider than the dimension of the zeolite nanocrystals, the analytical information about the Si/Al ratio is averaged over few zeolite nanocrystals and alumina matrix and corresponds to the bulk composition of the pellet. Reducing the spot diameter to the dimension close to zeolite nanocrystals detects increased Si/Al ratio when the spot hits a zeolite nanocrystal. The Si/Al ratio detected with spot of 5 nm reached a maximum between steps 3−5 and 7−10 (Figure 7). Hence, a zeolite phase in the form of separated zeolite nanocrystals of ~15 nm is consistent with HR-TEM data (Figure 6a,b). Since EDAX analysis collects information in three dimensions from the full particle depth, the SiO_2/Al_2O_3 ratio measured at these maximum points (steps 4 and 8) do not reach the value of 33.8, corresponding to pure zeolite β separated from colloidal solution. Attractive force between the alumina particles and zeolite nanocrystals in solution are high enough to desintegrate the nanocrystals' flocculates, yielding uniform distribution of zeolite nanocrystals in alumina.

The micropore volume and total surface area of zeolite phase in composite sample was calculated from the data presented in Table 1 assuming additivity of micropore volumes and surface areas of calcined pure zeolite phase and alumina matrix. The calculated value of 638 m^2/g ((473−320 × 0.52)/0.48) is very close to the total surface area of calcined zeolite β not incorporated in alumina matrix, evident for lack of blocking of the micropores and external surface of zeolite nanocrystals imbedded

(14) Newsam, J. M.; Treacy, M. M. J.; Koetsier, W.T.; Gruyter, C. B. *Proc. R. Soc. London* **1988**, *A420*, 375.

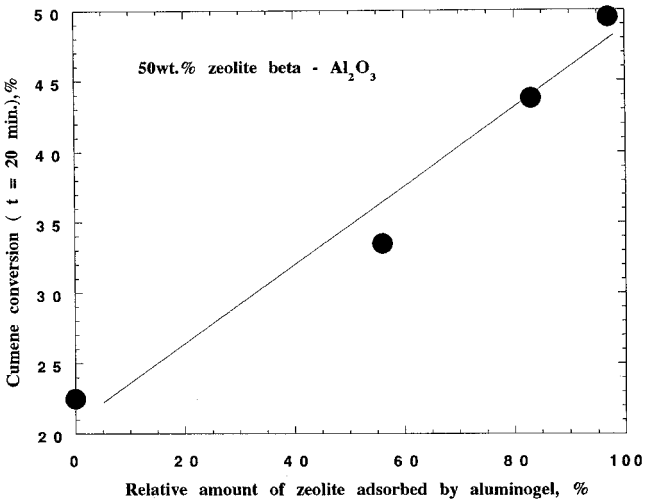

Figure 8. Effect of relative amount of zeolite β phase adsorbed by aluminogel on cumene conversion with 50 wt % zeolite−Al_2O_3 composite material.

in alumina matrix. The higher value of micropore volume of zeolite phase 0.210 cm^3/g ((0.12−0.039 × 0.52)/0.48) compared with calcined zeolite β not incorporated into alumina matrix (0.165 cm^3/g) is consistent. Some modification probably occurs in the texture of alumina matrix after incorporation the zeolite crystals that could explain an increase of calculated micropore volume without change in zeolite surface area.

A series of composite samples with zeolite content ranging from 28 to 80 wt % was prepared as described above by varying the pH of the mixed suspension from 11.8 to 10.0 at zeolite alumina ratio 1:1 and increasing the zeolite/alumina ratio at pH = 10.0. Up to zeolite content 58 wt % no clusters of zeolite β nanocrystals were detected by HR-TEM. At 80 wt %, zeolite loading clusters 30−40 nm in diameter appeared (Figure 8c) due to aggregation of adjucent zeolite nanocrystals during calcination of composite material at low alumina content.

Acidity Test. Catalytic activity in cumene cracking at conditions where the alumina matrix was fully inactive was employed. Three samples containing 50 wt % zeolite β in alumina matrix were prepared, varying the relative amount of zeolite phase adsorbed by aluminogel thus inhibiting nanocrystals aggregation. A fourth sample was prepared by mechanical mixing of powders at the same zeolite/Al_2O_3 ratio.

The cumene conversions measured with the four samples after 20 min of run are plotted in Figure 8. No adsorption during mechanical mixing of calcined components for the fourth sample was assumed. A nearly linear dependency was measured. Cumene conversion was twice as high in case of almost full adsorption of colloidal zeolite by aluminogel compared with mechanical mixing of the calcined components. The adsorption of colloidal zeolite β on aluminogel increased acidity of the zeolite phase after calcination compared with the same zeolite sample in form of calcined bulk nanozeolite clusters. This could be a result of different state of calcined zeolite β phase inside the alumina mesopores and in bulk clusters.

Comparison the State of Zeolite Phase in Bulk Clusters and Nanocrystals in Mesopores of Alumina Matrix. The TEA-containing material separated from colloidal solution by evaporation was calcined in air as has been previously described for composite material preparation. The material after calcination still consists of densely packed particles with narrow size (40−60 nm) distribution, according to SEM and HR-TEM analysis. It was not possible to detect separate zeolite nanocrystals inside the spherical particles (Figure 4b). They did not contain macropores and looked like single zeolite crystals with highly disordered domains and substantial disorder of atomic layered structure. The significantly larger particle size of dried sample is evident for sintering the nanozeolite clusters during calcination. Calcination removed the TEA template from the bulk dried zeolite β, so micropore volume became 0.165 cm^3/g and the total pore volume and BET surface area increased (Table 1) while the external surface area calculated from the slope of the t-plot of N_2 isotherm (300 m^2/g) remained unchanged. The N_2-desorption isotherm of calcined sample indicates a slight decrease of the large mesopores' diameter and an increase of the small 2−5-nm mesopores volume compared with dried sample (Figure 5, curve b). It reflects the increase of the packing density of zeolite nanocrystals in clusters after calcination. Calcination does not cause accretion of nanocrystals so that their micropore volume and external surface is not blocked after clusters sintering. The state of zeolite β nanocrystals in bulk clusters is then close to that in the mesopores of alumina matrix.

The WAXS patterns of the dried bulk zeolite β separated from colloidal solution are shown in Figure 9a, in agreement with refs 12 and 14. For the dried sample, the peak of 100% intensity was detected at 2θ = 22.45°, in agreement with Cambor et al.[12] After calcination, substantial widening and decrease of the peaks' intensity at 2θ >20° was observed, and the peak at 2θ = 7.87° became the most intensive (Figure 9b). It could indicate loss of long-range order in nanocrystals during calcination. A decrease in domain diameter, calculated according to Scherrer equation (peak 2θ = 22.45−22.55°), from 16.5 to 10.5 nm, could be evident for compression of primary zeolite nanocrystals after TEA removal. Shifting positions of peaks to higher 2θ values from 7.75 to 7.87° and from 22.45 to 22.53° reflects lattice contraction during calcination. With increasing zeolite content in calcined composite samples up to 58 wt %, the intensity of XRD peaks increased. Features of diffractograms were close to those detected for dried colloidal zeolite: the peak of 100% intensity was detected at 2θ = 22.45° and the low-angle peak position to 2θ = 7.64−7.73°. It indicates long-range order in zeolite nanocrystals imbedded in alumina matrix after calcination. Comparison of the peaks position with values obtained for bulk calcined zeolite sample separated from colloidal solution (22.45 and 7.87°) indicate less lattice contraction during calcination of zeolite crystals incorporated in alumina matrix. The Scherrer crystal diameter calculated based on the width of peak at 2θ = 22.22−22.37° was 6−8 nm in agreement with nanocrystals' diameter detected by HR-TEM, taking into account the possible peak widening as a result of X-ray scattering on alumina matrix. This effect could explain also very low intensities of the XRD peaks at diffraction angles 2θ >25°.

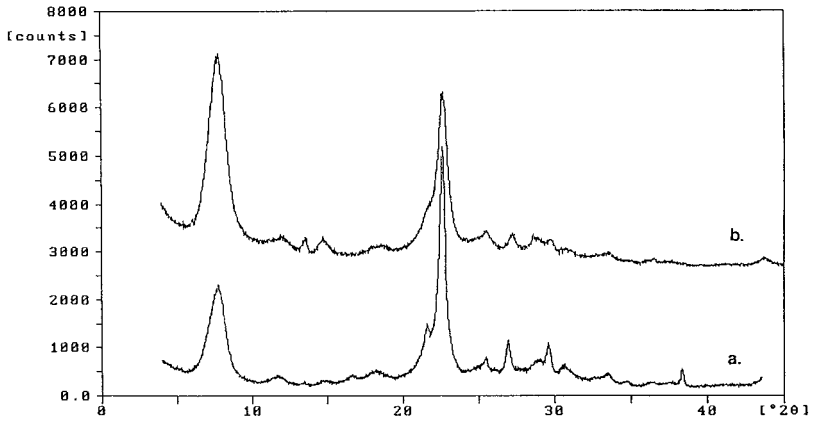

Figure 9. WAXS patterns of zeolite β separated from colloidal solution: (a) after drying at 100 °C and (b) after drying and calcination at 550 °C.

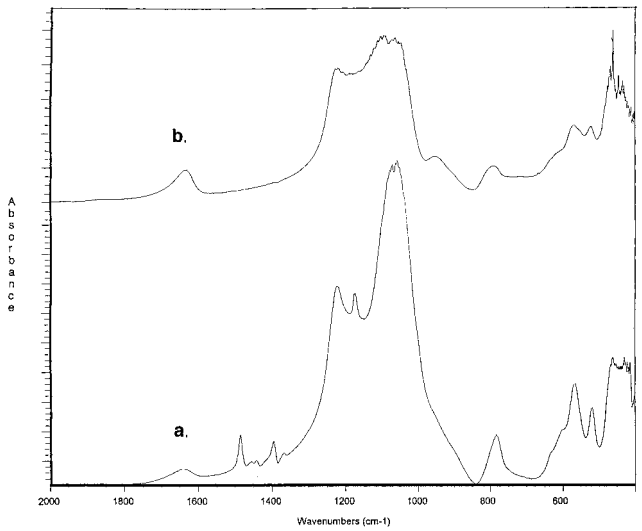

Figure 10. IR spectra of zeolite β separated from colloidal solution: (a) after drying at 100 °C and (b) after drying and calcination at 550 °C.

The pattern of IR spectra of the dried zeolite β separated from colloidal solution (Figure 10a) was characteristic of zeolite β. The well-resolved bands at 500−650 cm^{-1} indicate high order of zeolite bulk structure, and the shoulder at 900−950 cm^{-1}, terminal $Si-O^-$ groups located mainly at the external surface of nanocrystals in clusters.[12] The bands at 1000−1300 and 400−500 cm^{-1} correspond to valence and deformational vibrations inside SiO_4 tetrahedra. After calcination (Figure 10b), the sharp features in the region 500−650 cm^{-1} were widened and lowered in intensity. Widening and relative intensity changes of the bands in the 1000−1300 cm^{-1} range as well as alteration of the fine structure in 400−500 cm^{-1} range are observed. A clear band around 900−950 cm^{-1} emerged. These changes in the IR spectra could be related to tetrahedron disordering in the zeolite framework and formation of internal $Si-O^-$ defect groups due to low thermostability of zeolite β nanocrystals in bulk clusters detected recently in refs 13 and 15.

The IR spectra of the composite samples after calcination at 550 °C display an increase of the peaks intensity in 1000−1300 cm^{-1} range, corresponding to valence vibrations of the SiO_4 tetrahedra of zeolite β with increasing the zeolite content from 28 to 80 wt %. At zeolite loadings of 40−58 wt %, these peaks were comparatively sharp and did not change their shape with increasing the zeolite content. At lower wavenumbers, the bands of alumina masked the zeolite spectra especially at 900−980 cm^{-1} where alumina displayed a strong shoulder. However the bands at 500−650 cm^{-1} characteristic of zeolite structure were clearly observed at the background of alumina spectra. At 80 wt % zeolite loading, the IR features in the range of 1000−1300 cm^{-1} were widened. A peak at 950 cm^{-1} appeared, and the intensities of the peaks in the range of 500−650 cm^{-1} decreased compared with the sample of 58 wt % zeolite loading. Those data could be evident for stable structure order of zeolite β framework in nanocrystals imbedded in alumina matrix at loadings up to 60 wt %.

^{29}Si MAS NMR spectra of bulk and calcined zeolite β separated from colloidal solution are shown in parts a and b of Figure 11, respectively. Four different components centered at −104.8, −105.4, −109.9, and − 111.4 ppm can be distinguished in ^{29}Si spectra of as-synthesized sample. These components are deconvoluted in Figure 11a. After calcination, peaks at −99, −103, and −111 ppm were detected. In the ^{29}Si MAS NMR spectra of zeolite β the lines at chemical shifts <-110 ppm represent SiO_4 tetrahedral units surrounded by four Si atoms bonded by siloxane bonds—Si(4Si), and located at different crystallographic positions with different TOT angles.[16,17] The lines at chemical shifts >-106 ppm represent SiO_4 units surrounded by 3Si 1Al or 2Si 2Al.[17] After calcination, the ratio of summarized integral intensities of the lines centered at >106 ppm/<−110 ppm was ~0.26, about half the value reported by Perez-Pariente et al.[17] for calcined microcrystalline β with comparable Si/Al ratio. This would indicate that aluminum atoms leave the tetrahedral positions in zeolite framework during calcination of nanocrystal clusters. This results in the formation of $Si-O^-$ defects that are consistent with our IR data (Figure 11) and ^{27}Al MAS NMR data reported by Vaudry et al.[15] for zeolite β 50-nm nanocrystals. The low-resolution of the components in ^{29}Si MAS NMR spectra of calcined sample at chemical

(15) Vaudry, F.; Di Renzo, F.; Fajula, F.; Schulz, P. *J. Chem. Soc., Faraday Trans.* **1998**, *94* (4), 617.
(16) Fyfe, C. A.; Strobl, H.; Kokotailo, G. T.; Pasztor, C.T.; Barlow, G. E.; Bradley, S. *Zeolites* **1988**, *8*, 132.
(17) Perez-Pariente, J.; Sanz, J.; Fornes, V.; Corma, A. *J. Catal.* **1990**, *124*, 217.

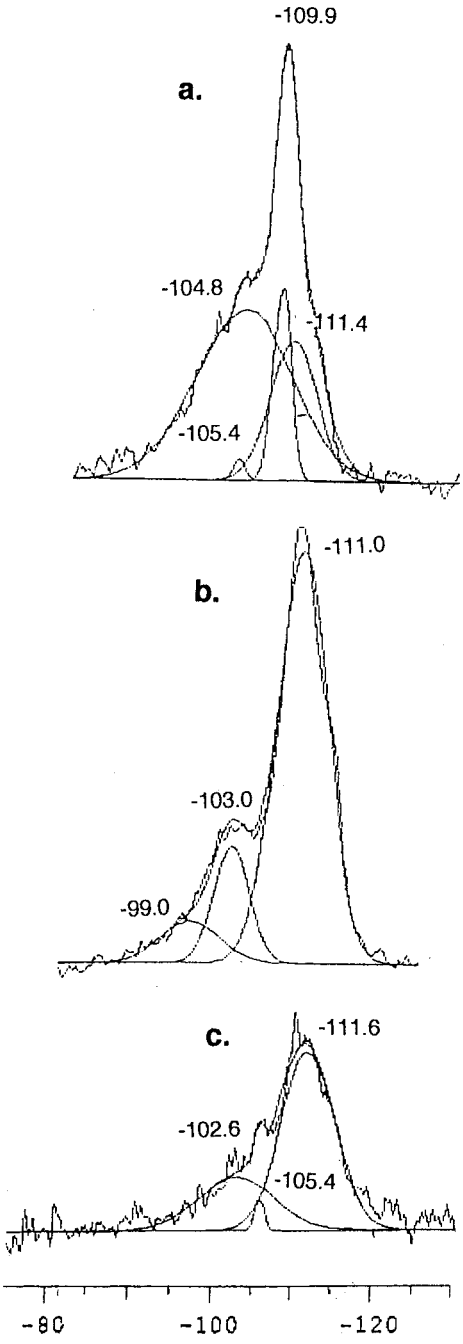

Figure 11. ^{29}Si MAS NMR spectra of zeolite β separated from colloidal solution and composite material zeolite $\beta-Al_2O_3$: (a) bulk zeolite β after drying at 100 °C; (b) bulk zeolite β after drying and calcination at 550 °C; and (c) 48 wt % zeolite $\beta-Al_2O_3$ pellets calcined at 550 °C.

shifts <-110 ppm could also indicate high concentration of silanol groups.[17]

The ^{29}Si MAS NMR spectra of calcined composite sample containing 48 wt % zeolite are shown in Figure 11c. The peaks centered at chemical shifts of >-106 ppm corresponding to SiO_4-Al_n units in zeolite framework remained after calcination compared with pure zeolite separated from colloidal solution. The ratio of the summarized integral intensities of the lines centered at >-106 ppm/<-110 ppm was ~0.48 compared with ~0.28 for bulk zeolite sample (Figure 11a). This is close to the value observed by Perez-Pariente et al.[17] for calcined microcrystalline zeolite β with close Si/Al ratio. This could be evident of the higher thermal stability of the zeolite framework structure in alumina matrix at optimal zeolite loadings compared with bulk nanozeolite clusters. However, since dried nanocrystals of zeolite β have Q^3 silica units at the external surface and may be the interior too (defined above as Si−O− defect groups), calcination and sintering can decrease these defect site concentration also affecting the shape of ^{29}Si MAS NMR spectra. Additional methods should be applied for direct measuring the concentration of tetrahedral aluminum atoms in zeolite β nanocrystals to make this question clear.

The improved catalytic performance and crystallographic quality of nanocrystal zeolite β incorporated in alumina matrix could be a result of several potential mechanisms: stabilization of nanocrystals from clusters formation and sintering; "chemical effects" like migration of aluminum atoms from the matrix to zeolite crystals and different compositions of zeolite materials treated at different pH; or partial destruction of zeolite nanocrystals at high alkalinity during evaporation the colloidal solution.

No definitive destinction among the various mechanisms can be made on the basis of the avilable data.

Conclusions

Spherical, 10−20 nm, nanocrystals of zeolite β were prepared in colloidal solution in equilibrium with water-rich flocculates. After separation, the zeolite material formed nanozeolite clusters of 60−100 nm containing mesopores. These clusters display low thermostability and undergo compression during calcination, forming "sintered clusters" of 40−60 nm in diameter with highly disordered structure. Incorporation of the colloidal zeolite β in alumina matrix does not block their external surface or internal volume. It inhibits their aggregation, increasing the thermal stability and acidity of the zeolite phase in alumina matrix mesopores. Stabilization of zeolite nanocrystals in the mesoporous alumina matrix is a viable method for testing the zeolite crystal size effects in catalysis at nanocrystal range.

Acknowledgment. This research was partially supported by the Israel Scientific Foundation founded by the Israel Academy of Sciences & Humanities. The authors thank Professor M. Talianker for valuable assistance in the HR-TEM and Dr. Tapas Sen for conducting the ^{29}Si MAS NMR. The authors also thank one of the reviewers for suggesting potential mechanisms mentioned in the paper.

CM980765U